Lattice QCD exploration of parton pseudo-distribution functions

Kostas Orginos,[1,2] Anatoly Radyushkin,[3,2] Joseph Karpie,[1,2] and Savvas Zafeiropoulos[1,2]

[1] *Department of Physics, The College of William & Mary, Williamsburg, VA 23187, USA*
[2] *Thomas Jefferson National Accelerator Facility, Newport News, VA 23606, USA*
[3] *Physics Department, Old Dominion University, Norfolk, VA 23529, USA*

We demonstrate a new method of extracting parton distributions from lattice calculations. The starting idea is to treat the generic equal-time matrix element $\mathcal{M}(Pz_3, z_3^2)$ as a function of the Ioffe time $\nu = Pz_3$ and the distance z_3. The next step is to divide $\mathcal{M}(Pz_3, z_3^2)$ by the rest-frame density $\mathcal{M}(0, z_3^2)$. Our lattice calculation shows a linear exponential z_3-dependence in the rest-frame function, expected from the $Z(z_3^2)$ factor generated by the gauge link. Still, we observe that the ratio $\mathcal{M}(Pz_3, z_3^2)/\mathcal{M}(0, z_3^2)$ has a Gaussian-type behavior with respect to z_3 for 6 values of P used in the calculation. This means that $Z(z_3^2)$ factor was canceled in the ratio. When plotted as a function of ν and z_3, the data are very close to z_3-independent functions. This phenomenon corresponds to factorization of the x- and $k_\perp$-dependence for the TMD $\mathcal{F}(x, k_\perp^2)$. For small $z_3 \leq 4a$, the residual z_3-dependence is explained by perturbative evolution, with $\alpha_s/\pi = 0.1$.

PACS numbers: 12.38.-t, 11.15.Ha, 12.38.Gc

arXiv:1706.05373v4 [hep-ph] 27 Oct 2017

I. INTRODUCTION

Extraction of parton distribution functions (PDFs) $f(x)$ [1] on the lattice is a challenging problem attracting a lot of attention. The usual method to approach PDFs on the lattice is to calculate their moments. However, recently, X. Ji [2] suggested a method allowing a calculation of PDFs as functions of x.

Since the PDFs are related to matrix elements of bilocal operators on the light cone $z^2 = 0$, this was a stumbling block preventing a direct calculation of these functions in the lattice gauge theory formulated in Euclidean space.

To overcome this difficulty, X. Ji proposes to use purely space-like separations $z = (0, 0, 0, z_3)$. The functions in this case are quasi-PDFs $Q(y, p_3)$ describing the distribution of the p_3 hadron momentum component. The key point is that quasi-PDFs $Q(y, p_3)$ tend to usual PDFs $f(y)$ in the $p_3 \to \infty$ limit. The same method can be applied to distribution amplitudes (DAs). The results of quasi-PDF calculations on the lattice were reported in Refs. [3–5] and of the pion quasi-DA in Ref. [6].

Recent papers [7, 8] by one of the authors (A.R.) contain an investigation of the nonperturbative p_3-evolution of quasi-PDFs and quasi-DAs. This study is based on the formalism of virtuality distribution functions [9, 10]. The approach developed in Refs. [7, 8] has established a connection between the quasi-PDFs and the "straight-link" transverse momentum dependent distributions (TMDs) $\mathcal{F}(x, k_\perp^2)$. Starting from simple models for TMDs, models were built for the nonperturbative evolution of quasi-PDFs. The derived curves agree qualitatively with the patterns of p_3-evolution produced by lattice simulations.

The structure of quasi-PDFs was further studied in Ref. [11]. It was shown that, when a hadron is moving, the parton k_3 momentum may be treated as coming from two sources. The hadron's motion as a whole yields the xp_3 part, which is governed by the dependence of the TMD $\mathcal{F}(x, \kappa^2)$ on its first argument namely x. The residual part $k_3 - xp_3$ is controlled by the way that the TMD depends on its second argument, κ^2, which dictates the shape of the primordial rest-frame momentum distribution. Quasi-PDFs due to their convolution nature possess a rather involved pattern of their p_3-evolution, making mandatory relatively big values $p_3 \gtrsim 3$ GeV in order to safely approach the PDF limit.

To accelerate the convergence, a different approach for the PDF extraction from lattice calculations was proposed [11]. It is based on the concept of *pseudo-PDFs* $\mathcal{P}(x, z_3^2)$. They generalize the light-cone PDFs $f(x)$ onto spacelike intervals like $z = (0, 0, 0, z_3)$. The pseudo-PDFs are Fourier transforms of the *Ioffe-time* [12] *distributions* [13] $\mathcal{M}(\nu, z_3^2)$ which are generically given by matrix elements $\langle p|\phi(0)\phi(z)|p\rangle$ written as functions of $\nu = p_3 z_3$ and z_3^2. In contrast to quasi-PDFs, the pseudo-PDFs have the "canonical" $-1 \leq x \leq 1$ support for all values of z_3^2. In the limit $z_3 \to 0$ they tend to PDFs, showing, in this limit, a typical perturbative evolution with the scale $1/z_3$ being the parameter of evolution.

As discussed in [7, 8], the fast nonperturbative decrease with z_3^2 of the pseudo-PDFs $\mathcal{P}(x, z_3^2)$ or the Ioffe-time distribution $\mathcal{M}(\nu, z_3^2)$, is responsible for delaying the approach of quasi-PDFs $Q(y, p_3)$ to the PDF $f(y)$. An important observation is that one can strongly reduce the z_3^2-dependence by simply dividing the Ioffe-time distribution $\mathcal{M}(\nu, z_3^2)$ by an appropriate factor $D(z_3^2)$ satisfying $D(0) = 1$ and having the z_3^2-dependence close (on average) to that of $\mathcal{M}(\nu, z_3^2)$. The absence of the ν-dependence in this factor and its $D(0) = 1$ normalization guarantees that the ratio $\mathcal{M}(\nu, z_3^2)/D(z_3^2)$ taken in the $z_3^2 \to 0$ limit will produce the same PDF as the original function $\mathcal{M}(\nu, z_3^2)$ taken in the same limit.

The choice for $D(z_3^2)$ advocated in Ref. [11], is to take it to be equal to the rest-frame function $\mathcal{M}(0, z_3^2)$. An additional advantage of this choice is that both $\mathcal{M}(\nu, z_3^2)$ and $\mathcal{M}(0, z_3^2)$ contain the same multiplicative

factor $Z(z_3^2)$ generated by the renormalization of the gauge link. In the ratio, it should cancel out.

Our goal in the present work is an exploratory lattice calculation of the u-d proton PDF using the strategy outlined in Ref. [11]. To make this article self-contained, we reproduce in Sections II and III the main ideas of Ref. [11]. The description of the method used for the lattice extraction of the reduced Ioffe-time distribution is given in Section IV. The data analysis and interpretation is discussed in Section V. The summary of the paper is given in Section VI.

II. PARTON DISTRIBUTIONS

A. Generic matrix element and parton distributions

The basic object for defining parton distributions is a matrix element of a bilocal operator that (skipping inessential details of its spin structure) may be written generically like $\langle p|\phi(0)\phi(z)|p\rangle$. Due to invariance under Lorentz transformations, it is given by a function of two scalars, (pz) (which will be denoted by $-\nu$) and z^2 (or $-z^2$, in order to have a positive value for spacelike z)

$$\langle p|\phi(0)\phi(z)|p\rangle = \mathcal{M}(-(pz),-z^2) = \mathcal{M}(\nu,-z^2)\,. \tag{1}$$

One can demonstrate [7, 14] that, for all relevant Feynman diagrams, its Fourier transform $\mathcal{P}(x,-z^2)$ with respect to (pz) has $-1\le x\le 1$ as support, i.e.,

$$\mathcal{M}(-(pz),-z^2) = \int_{-1}^{1} dx\, e^{-ix(pz)}\,\mathcal{P}(x,-z^2)\ . \tag{2}$$

Eq. (2) serves as a covariant definition of x. In this definition of x, one does not need to assume that $p^2=0$ or $z^2=0$.

Choosing a light-like z, e.g., having solely the light-front component z_-, we parametrize the matrix element by $f(x)$, the twist-2 parton distribution

$$\mathcal{M}(-p_+z_-,0) = \int_{-1}^{1} dx\, f(x)\, e^{-ixp_+z_-}\ . \tag{3}$$

One can rewrite this definition as

$$\mathcal{M}(\nu,0) = \int_{-1}^{1} dx\, f(x)\, e^{ix\nu}\ . \tag{4}$$

The inverse relation is given by

$$f(x) = \frac{1}{2\pi}\int_{-\infty}^{\infty} d\nu\, e^{-ix\nu}\,\mathcal{M}(\nu,0) = \mathcal{P}(x,0)\ . \tag{5}$$

Due to the fact that $f(x)=\mathcal{P}(x,0)$, the function $\mathcal{P}(x,-z^2)$ provides a generalization of the concept of PDFs onto non-lightlike intervals z^2 (in principle, z^2 may be even timelike). Following [11] , we will be referring to it as the *pseudo-PDF*. The variable $(pz)=-\nu$ is called often the *Ioffe time* [12], and consequently $\mathcal{M}(\nu,-z^2)$ is the *Ioffe-time distribution* [13].

In renormalizable theories (including QCD), the function $\mathcal{M}(\nu,-z^2)$ has logarithmic $\sim \ln(-z^2)$ singularities which generate the perturbative evolution of parton densities. In the approach based on the operator product expansion (OPE), the standard procedure is to remove these singularities with the help of some prescription. The most popular of them is the $\overline{\rm MS}$ scheme based on dimensional regularization. Consequently the resulting PDFs have a dependence on the renormalization scale μ, and therefore one should write the PDFs as $f(x,\mu^2)$.

At small spacelike z^2 and at the leading logarithm level, the pseudo-PDFs are related to the $\overline{\rm MS}$ distributions by a simple rescaling of their second arguments. In particular, when $z^2=-z_3^2$, one has

$$\mathcal{P}(x,z_3^2) = f\left(x,(2e^{-\gamma_E}/z_3)^2\right)\ , \tag{6}$$

where γ_E is the Euler's constant. The rescaling factor between μ and $1/z_3$ is very close to 1, since $2e^{-\gamma_E}=1.12$.

B. Transverse momentum dependent- and quasidistributions

Treating the target momentum p as longitudinal, $p=(E,\mathbf{0}_\perp,P)$, one can introduce transverse degrees of freedom. In particular, taking z that has z_- and $z_\perp=\{z_1,z_2\}$ components only, one defines the *TMD* $\mathcal{F}(x,k_\perp^2)$

$$\mathcal{P}(x,z_\perp^2) = \int d^2\mathbf{k}_\perp e^{i(\mathbf{k}_\perp\mathbf{z}_\perp)}\mathcal{F}(x,k_\perp^2)\ . \tag{7}$$

In this context, the pseudo-PDFs $\mathcal{P}(x,z_\perp^2)$ actually coincide with the *impact parameter distributions*, a familiar object used in many TMD studies.

Since one cannot arrange light-like separations on the lattice, it was proposed [2] to consider equal-time spacelike separations $z=(0,0,0,z_3)$ (or, for brevity, $z=z_3$). Then, in the $p=(E,0_\perp,P)$ frame, one can introduce the quasi-PDF $Q(y,P)$ through a parametrization

$$\langle p|\phi(0)\phi(z_3)|p\rangle = \int_{-\infty}^{\infty} dy\, Q(y,P)\, e^{iyPz_3}\ . \tag{8}$$

According to this definition, the quasi-PDF $Q(y,P)$ describes the probability that the parton carries the fraction y of the parent hadron's third momentum component P. The variables ν and $-z^2$ in this case are given by Pz_3 and z_3^2, so we have

$$\mathcal{M}(\nu,z_3^2) = \int_{-\infty}^{\infty} dy\, Q(y,P)\, e^{iy\nu}\ . \tag{9}$$

Since $z_3^2=\nu^2/P^2$, the inverse Fourier transformation may be written as

$$Q(y,P) = \frac{1}{2\pi}\int_{-\infty}^{\infty} d\nu\ e^{-iy\nu}\,\mathcal{M}(\nu,\nu^2/P^2)\ . \tag{10}$$

It shows that $Q(y,P)$ tends to $f(y)$ in the $P\to\infty$ limit, since formally $\mathcal{M}(\nu,\nu^2/P^2)\to\mathcal{M}(\nu,0)$ when $P\to\infty$.

As established in Ref. [7], quasi-PDFs may be written in terms of TMDs

$$Q(y,P)/P=\int_{-\infty}^{\infty}dk_1\int_{-1}^{1}dx\,\mathcal{F}(x,k_1^2+(y-x)^2P^2)\ . \tag{11}$$

C. Quantum chromodynamics (QCD) case

In case of the non-singlet parton densities of QCD, one is considering matrix elements

$$\mathcal{M}^\alpha(z,p)\equiv\langle p|\bar\psi(0)\,\gamma^\alpha\,\hat E(0,z;A)\psi(z)|p\rangle\ , \tag{12}$$

where $\hat E(0,z;A)$ is the standard $0\to z$ straight-line gauge link in the quark (fundamental) representation. These matrix elements can be decomposed into p^α and z^α parts

$$\mathcal{M}^\alpha(z,p)=2p^\alpha\mathcal{M}_p(-(zp),-z^2)+z^\alpha\mathcal{M}_z(-(zp),-z^2)\ . \tag{13}$$

Only the $\mathcal{M}_p(-(zp),-z^2)$ part gives the twist-2 distribution when $z^2\to0$.

Introducing TMDs, one takes $z=(z_-,z_\perp)$ and the $\alpha=+$ component of $\mathcal{M}^\alpha$. Hence, the z^α-part drops out. After that, $\mathcal{M}_p(\nu,z_\perp^2)$ is the only surviving part of $\mathcal{M}^\alpha(z,p)$, and in the remaining discussion we use the short hand notation of $\mathcal{M}\equiv\mathcal{M}_p$.

In the case of quasidistributions $Q(y,P)$, we can avoid the z^α contamination by considering the time component of $\mathcal{M}^\alpha(z=z_3,p)$ and defining

$$\mathcal{M}^0(z_3,p)=2p^0\int_{-1}^{1}dy\,Q(y,P)\ e^{iyPz_3}\ . \tag{14}$$

D. Factorized models

The structure of the quasi-PDFs may be illustrated on the example of the simplest models in which the nonperturbative (or soft) part of the TMDs $\mathcal{F}(x,k_\perp^2)$ is represented by a product

$$\mathcal{F}^{\rm soft}(x,k_\perp^2)=f(x)K(k_\perp^2) \tag{15}$$

of the collinear parton distribution $f(x)$ and a $k_\perp^2$-dependent factor $K(k_\perp^2)$, usually modeled by a Gaussian. As we shall see, the quasi-PDFs have a rather complicated structure, even when they are built from these simple factorized models.

For the Ioffe-time distribution $\mathcal{M}(\nu,-z^2)$, this Ansatz corresponds to the factorization assumption

$$\mathcal{M}^{\rm soft}(\nu,z_3^2)=\mathcal{M}^{\rm soft}(\nu,0)\mathcal{M}(0,z_3^2) \tag{16}$$

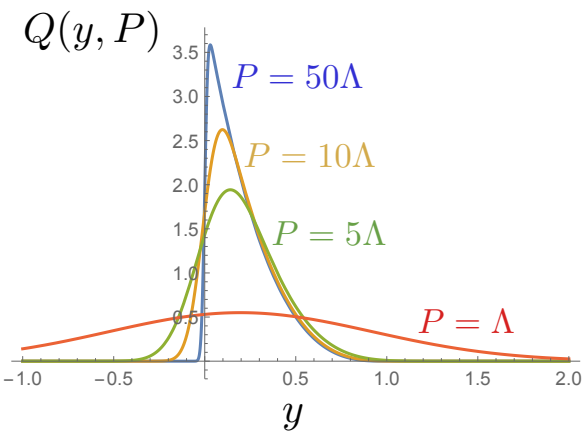


FIG. 1. Evolution of quasi-PDF $Q(y,P)$ in the factorized Gaussian model for $P/\Lambda=1,5,10,50$.

for its soft part. Still, even if the soft TMD factorizes, the soft part of the quasi-PDF has the convolution structure of Eq. (11). Taking, for example, a Gaussian form

$$K_G(k_\perp^2)=\frac{1}{\pi\Lambda^2}e^{-k_\perp^2/\Lambda^2}\ , \tag{17}$$

one gets the following model for the quasi-PDF

$$Q_G(y,P)=\frac{P}{\Lambda\sqrt{\pi}}\int_{-1}^{1}dx\,f(x)\,e^{-(x-y)^2P^2/\Lambda^2}\ . \tag{18}$$

Choosing for $f(x)$ a simple toy PDF resembling the nucleon valence densities $f(x)=4(1-x)^3\theta(0\le x\le1)$, one gets the curves shown in Fig. 1. For large P, the quasi-PDF clearly tends to the $f(y)$ PDF form. However, only for $P\sim10\Lambda$ one gets a quasi-PDF that is rather close to the $P\to\infty$ limiting shape. Still, since $\Lambda\sim\langle k_\perp\rangle$, one translates the $P\sim10\Lambda$ estimate into $P\sim3$ GeV, which is rather large.

III. PSEUDO-PDFS

The involved structure of a quasi-PDF $Q(y,P)$ can be attributed to the formal fact that it is given by the Fourier ν-transform of the function $\mathcal{M}(\nu,\nu^2/P^2)$, in which ν appears both in the first and second argument of the Ioffe-time distribution. One should take P-values that are sufficiently large to neglect the ν-dependence coming from the second argument.

Another way [11] is to try to *eliminate* the z_3^2-dependence induced by $\mathcal{M}(\nu,z_3^2)$. The main idea is based on the observation that if one takes the ν-Fourier transform of the modified function $\mathcal{M}(\nu,z_3^2)/D(z_3^2)$, the $z_3\to0$ limit will give the same PDF as the original Ioffe-time distribution, provided that $D(z_3^2)$ is a function of z_3^2 only (but not of ν) and is equal to 1 for $z_3^2=0$.

Thus, the strategy is to find a function $D(z_3^2)$ whose z_3^2-dependence would compensate, as much as possible,

the z_3^2-dependence of $\mathcal{M}(\nu, z_3^2)$. The next step is to fit the residual polynomial z_3^2-dependence by polynomials of z_3^2 (they may be different for different values of ν), and in this way extrapolate the data to $z_3^2 = 0$ limit. The Fourier transform of the resulting function would correspond to the same PDF as the z_3^2 limit of the original Ioffe-time distribution $\mathcal{M}(\nu, z_3^2)$.

In the most lucky situation, the ratio $\mathcal{M}(\nu, z_3^2)/D(z_3^2)$ would have no polynomial z_3^2-dependence (or just a very mild one). In particular, when $\mathcal{M}(\nu, z_3^2)$ factorizes, i.e., $\mathcal{M}(\nu, z_3^2) = \mathcal{M}(\nu, 0)\mathcal{M}(0, z_3^2)$, one should take $D(z_3^2) = \mathcal{M}(0, z_3^2)$. In this case, the reduced function

$$\mathfrak{M}(\nu, z_3^2) \equiv \frac{\mathcal{M}(\nu, z_3^2)}{\mathcal{M}(0, z_3^2)} \tag{19}$$

is equal to $\mathcal{M}(\nu, 0)$, and the task of obtaining the $z_3 \to 0$ limit is accomplished.

While there is no "first principle" reason for such a factorization, one may expect that the functions $\mathcal{M}(\nu, z_3^2)$ for different ν have more or less similar dependence on z_3, basically reflecting the finite size of the nucleon.

As we mentioned already, the soft part of $\mathcal{M}(\nu, z_3^2)$ factorizes if the soft part of TMD $\mathcal{F}(x, k_\perp^2)$ factorizes. That this happens, is a standard assumption of the TMD practitioners (see, e.g., Ref. [15]). So, there are good chances that this part of the z_3^2-dependence of $\mathcal{M}(\nu, z_3^2)$ will be canceled or strongly reduced by the rest-frame function $\mathcal{M}(0, z_3^2)$.

On the lattice, there is another (and troublesome, see, e.g., Ref. [16]) source of z_3-dependence: the $Z(z_3^2)$ factor generated by the renormalization of the gauge link $\hat{E}(0, z_3; A)$. Fortunately, this problematic factor $Z(z_3^2)$ does not depend on ν and is the same for the numerator and denominator of the ratio $\mathfrak{M}(\nu, z_3^2)$. This provides another motivation for using $\mathcal{M}(0, z_3^2)$ as a factor $D(z_3^2)$.

Thus, the proposal is to perform a lattice study of the reduced Ioffe-time function $\mathfrak{M}(\nu, z_3^2)$. Even if it would have a residual polynomial z_3^2-dependence, it should be much easier to extrapolate this dependence to $z_3 = 0$, than the z_3-dependence of the original Ioffe-time distribution $\mathcal{M}(\nu, z_3^2)$.

Furthermore, if one observes that the ratio $\mathfrak{M}(\nu, z_3^2)$ does not have z_3-dependence, one should conclude that $\mathcal{M}(\nu, z_3^2)$ factorizes. In fact, such a factorization has been already observed several years ago in the pioneering study [17] of the transverse momentum distributions in lattice QCD.

Still, there is an unavoidable source of factorization breaking. When z_3 is small, $\mathcal{M}(\nu, z_3^2)$ has logarithmic $\ln z_3^2$ singularities generating the perturbative evolution of PDFs. As we discussed, $1/z_3$ is analogous then to the renormalization parameter μ of the scale-dependent PDFs $f(x, \mu^2)$ within the standard OPE approach.

More specifically, for small values of z_3, the pseudo-PDF $\mathcal{P}(x, z_3^2)$ satisfies a leading-order evolution equation with respect to $1/z_3$ that is identical to the evolution equation for $f(x, \mu^2)$ with respect to μ. The evolution

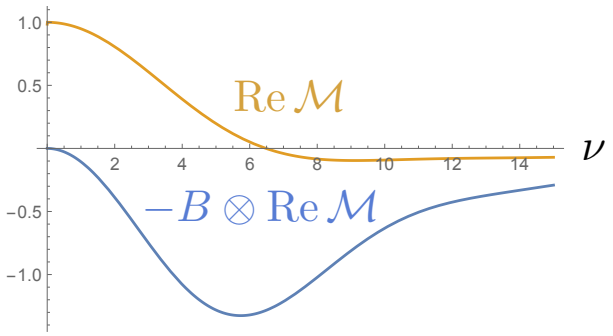


FIG. 2. Real part of model distribution $\mathcal{M}(\nu)$ and the function $-B \otimes \mathrm{Re}\,\mathcal{M}$ that governs its evolution (the minus sign here is for convenience of placing two curves on one figure).

equation for the reduced Ioffe-time distribution $\mathfrak{M}(\nu, z_3^2)$ can also be written [11]

$$\frac{d}{d \ln z_3^2} \mathfrak{M}(\nu, z_3^2) = -\frac{\alpha_s}{2\pi} C_F \int_0^1 du\, B(u) \mathfrak{M}(u\nu, z_3^2), \tag{20}$$

where $C_F = 4/3$, and the leading-order evolution kernel $B(u)$ for the non-singlet quark case is given [13] by

$$B(u) = \left[\frac{1+u^2}{1-u}\right]_+ , \tag{21}$$

where $[\ldots]_+$ denotes the "plus" prescription, i.e.

$$\int_0^1 du \left[\frac{1+u^2}{1-u}\right]_+ \mathfrak{M}(u\nu) = \int_0^1 du \frac{1+u^2}{1-u} \left[\mathfrak{M}(\nu) - \mathfrak{M}(u\nu)\right] . \tag{22}$$

Note that being a Fourier transform,

$$\mathcal{M}(\nu) = \int_{-1}^1 dx\, f(x)\, e^{ix\nu} , \tag{23}$$

the Ioffe-time distribution has real and imaginary parts even if the function $f(x)$ is real (which is the case with parton distributions). In particular,

$$\mathrm{Re}\,\mathcal{M}(\nu) = \int_{-1}^1 dx\, f(x)\, \cos(x\nu) , \tag{24}$$

and

$$\mathrm{Im}\,\mathcal{M}(\nu) = \int_{-1}^1 dx\, f(x)\, \sin(x\nu) . \tag{25}$$

In Fig. 2, we show the function $\mathrm{Re}\,\mathcal{M}(\nu)$ for a model PDF

$$q(x) = \frac{315}{32}\sqrt{x}(1-x)^3\theta(0 \le x \le 1) . \tag{26}$$

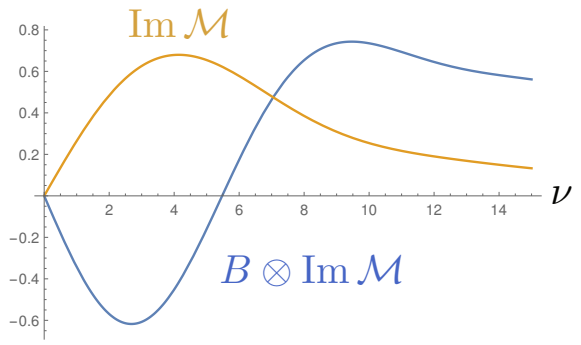


FIG. 3. Imaginary part of model Ioffe-time distribution $\mathcal{M}(\nu)$ and the function $B \otimes \mathrm{Im}\,\mathcal{M}$ that governs its evolution.

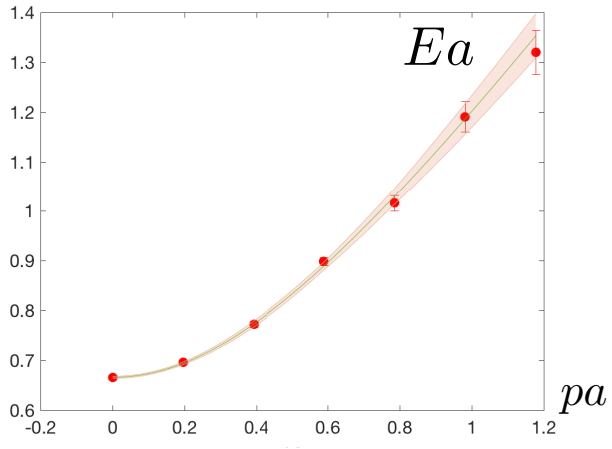


FIG. 4. Nucleon dispersion relation. Energies and momenta are in lattice units. The solid line is the continuum dispersion relation (not a fit) while the errorband is an indication of the statistical error of the lattice nucleon energies.

Its integral is normalized to 1, and it is nonzero for positive x only, which corresponds to the absence of antiquarks. As we shall see, this particular form appears in the description of actual lattice data. In Fig. 3, we show the function $\mathrm{Im}\,\mathcal{M}(\nu)$ for the same model PDF.

We also show in these figures the convolution integrals governing the evolution, namely $-B \otimes \mathrm{Re}\,\mathcal{M}(\nu)$ and $B \otimes \mathrm{Im}\,\mathcal{M}(\nu)$. The reader can notice that $B \otimes \mathcal{M}(\nu)$ is zero for $\nu = 0$, resulting from the vector current conservation. As a consequence, the perturbative evolution leaves the rest-frame density $\mathcal{M}(0, z_3^2)$ (which is always real) unaffected. In other words, the $\ln z_3^2$ terms are present only in the numerator $\mathcal{M}(\nu, z_3^2)$ of the $\mathfrak{M}(\nu, z_3^2)$ ratio, but not in its $\mathcal{M}(0, z_3^2)$ denominator.

Note also that the evolution of the real part always leads to a *decrease* of $\mathrm{Re}\,\mathcal{M}(\nu, z_3^2)$ when z_3^2 increases. For the imaginary part, the evolution pattern is more complicated. Namely, below $\nu \sim 5.5$, the function $\mathrm{Im}\,\mathcal{M}(\nu, z_3^2)$ *increases* when z_3^2 increases. Only above $\nu \sim 5.5$, the evolution leads to a decrease of $\mathrm{Im}\,\mathcal{M}(u\nu, z_3^2)$ with z_3^2, and the evolution pattern becomes similar to that of the real part.

IV. NUMERICAL INVESTIGATION

In order to check numerically the ideas discussed above we performed lattice QCD calculations in the quenched approximation at $\beta = 6.0$ on $32^3 \times 64$ lattices (lattice spacing $a = 0.093$ fm). We used the non-perturbatively tuned clover fermion action with the clover coefficients computed by the Alpha collaboration [18].

We used a total of 500 configurations separated by 1000 updates each one consisting of four over-relaxation and one heatbath sweeps. On each configuration we computed correlation functions from 6 randomly selected point sources. The pion and nucleon masses in this setup were determined to be 601(1) MeV and 1411(4)MeV respectively. Conversion to physical energy units was performed used the Alpha collaboration scale setting for quenched QCD [19].

Our nucleon states were boosted up to a total momentum of 2.5 GeV (corresponding to the 6th lattice momentum). Inside this momentum range, the continuum dispersion relation for the nucleon was satisfied within the errors of the calculation, indicating small lattice artifacts of $\mathcal{O}(aP)$. In Fig. 4 we plot the nucleon energy as a function of momentum along with the continuum dispersion relation corresponding to our lattice nucleon zero momentum energy.

The computation of the matrix elements was performed using the methodology described in [20] with an operator insertion given by Eq. (12). Taking the time component of the current we can isolate $\mathcal{M}_p(-z \cdot p, -z^2)$ which as discussed above is directly related to PDFs.

Following [20] we need to compute two types of correlation functions. The first is a regular nucleon two point function given by

$$C_P(t) = \langle \mathcal{N}_P(t) \overline{\mathcal{N}}_P(0) \rangle \,, \tag{27}$$

where $\mathcal{N}_P(t)$ is a helicity averaged, non-relativistic nucleon interpolating field with momentum p. The quark fields in $\mathcal{N}_p(t)$ are smeared with a gauge invariant Gaussian smearing. This choice of an interpolation field is known to couple well to the nucleon ground state (see discussion in [20]). The quark smearing width was optimized to give good overlap with the nucleon ground state within the range of momenta in our calculation. The second correlator is given by

$$C_P^{\mathcal{O}^0(z)}(t) = \sum_\tau \langle \mathcal{N}_P(t) \mathcal{O}^0(z, \tau) \overline{\mathcal{N}}_P(0) \rangle \,, \tag{28}$$

where

$$\mathcal{O}^0(z, t) = \overline{\psi}(0, t) \gamma^0 \tau_3 \hat{E}(0, z; A) \psi(z, t) \,, \tag{29}$$

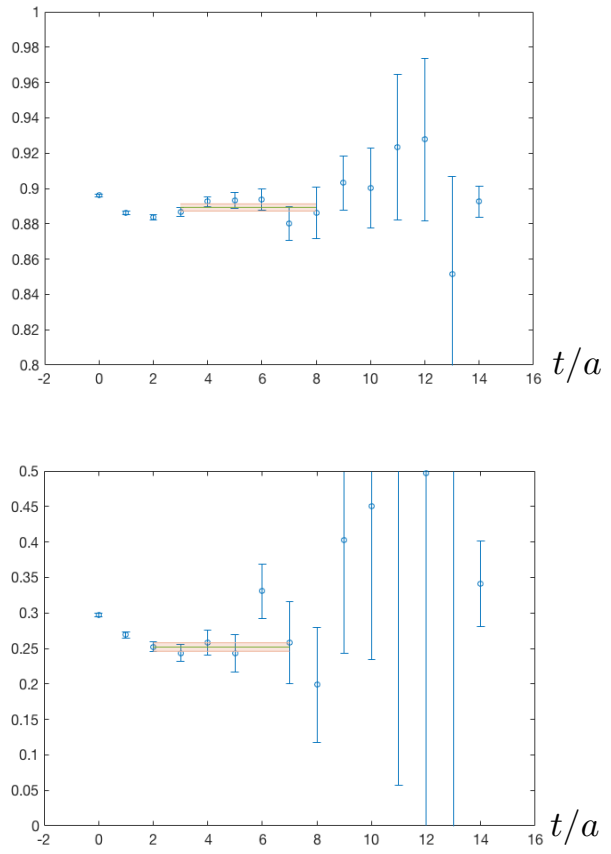


FIG. 5. Typical fits used to extract the reduced matrix element. The upper panel corresponds to $p = 2\pi/L \cdot 2$ and $z = 4$ and the lower panel to $p = 2\pi/L \cdot 3$ and $z = 8$, where momentum and position are in lattice units.

with τ_3 being the flavor Pauli matrix. The proton momentum and the displacement of the quark fields were both taken along the $\hat{z}$ axis ($\vec{z} = z_3\hat{z}$ and $\vec{p} = P\hat{z}$). We define the effective matrix element as

$$\mathcal{M}_{\text{eff}}(z_3P, z_3^2; t) = \frac{C_P^{\mathcal{O}^0(z)}(t+1)}{C_P(t+1)} - \frac{C_P^{\mathcal{O}^0(z)}(t)}{C_P(t)} \ . \quad (30)$$

As it was shown in [20], our matrix element $\mathcal{J}$ can then be extracted at the large Euclidean time separation as

$$\frac{\mathcal{J}(z_3P, z_3^2)}{2E} = \lim_{t\to\infty} \mathcal{M}_{\text{eff}}(z_3P, z_3^2; t) \ , \quad (31)$$

where E is the energy of the nucleon. This method of extracting the matrix element, contrary to the traditional sequential source approach, allows for the computation of the matrix element using all source-sink separations for the nucleon creation and annihilation operators.

The resulting effective matrix element has contaminations from excited states that scale as $e^{-t\Delta E}$, where t is the Euclidean time separation of the nucleon creation and annihilation operators, and ΔE is the mass gap to the first excited state of the nucleon. Furthermore, it allows for the computation of all nucleon matrix elements that correspond to different nucleon momentum spin polarization and flavor structure without additional computational cost.

As a result, the total computational cost of this approach is less than the equivalent cost of performing the calculations with the sequential source method, especially because in our approach we put emphasis on having as many nucleon momentum states as possible. This approach has recently been successfully used for both single and multi-nucleon matrix element calculations [21–23].

In order to normalize our lattice matrix elements we note that, for $z_3 = 0$, the matrix element $\mathcal{M}(z_3P, z_3^2)$ corresponds to a local vector (iso-vector) current, and therefore should be equal to 1. However, on the lattice this is not the case due to lattice artifacts. Therefore we introduce a renormalization constant

$$Z_P = \frac{1}{\mathcal{J}(z_3P, z_3^2)|_{z_3=0}} \ . \quad (32)$$

The factor Z_P has to be independent from P. However, again due to lattice artifacts or potential fitting systematics, this is not the case. For this reason, we renormalize the matrix element for each momentum with its own Z_P factor taking this way advantage of maximal statistical correlations to reduce statistical errors, as well as the cancellation of lattice artifacts in the ratio. Therefore, our matrix element is extracted using the ratio

$$\mathcal{M}(z_3P, z_3^2) = \lim_{t\to\infty} \frac{\mathcal{M}_{\text{eff}}(z_3P, z_3^2; t)}{\mathcal{M}_{\text{eff}}(z_3P, z_3^2; t)|_{z_3=0}} \ . \quad (33)$$

In order to determine the reduced matrix element $\mathfrak{M}(\nu, z_3^2)$ we introduce the double ratio

$$\mathfrak{M}(\nu, z_3^2) = \lim_{t\to\infty} \frac{\mathcal{M}_{\text{eff}}(z_3P, z_3^2; t)}{\mathcal{M}_{\text{eff}}(z_3P, z_3^2; t)|_{z_3=0}} \times \frac{\mathcal{M}_{\text{eff}}(z_3P, z_3^2; t)\big|_{P=0,z_3=0}}{\mathcal{M}_{\text{eff}}(z_3P, z_3^2; t)|_{P=0}} \ , \quad (34)$$

which takes care of the renormalization of the vector current according to Eq. (32). In practice, the infinite t limit is obtained with a fit to a constant for a suitable choice of a fitting range. In all cases we studied, the average χ^2 per degree of freedom was $\mathcal{O}(1)$. Typical fits used to extract the reduced matrix element are presented in Fig. 5. All fits are performed with the full covariance matrix and the error bars are determined with the jackknife method.

We note here that that the reduced matrix element defined in Eq. (34) has a well defined continuum limit and no additional renormalization is required. This continuum limit is obtained at fixed ν and z^2 as well as at fixed quark mass.

In this calculation we used momenta up to $6 \cdot 2\pi/L$ along the z-axis. This corresponds to a physical momentum of about 2.5 GeV.

V. DISCUSSION OF RESULTS

A. Rest-frame density and Z factor

An important object is the rest-frame density $\mathcal{M}(0, z_3^2)$. It is produced by data at $P = 0$. The results for its imaginary part are compatible with zero, as required. The real part, shown in Fig. 6, is a symmetric function of z_3, and has a clearly visible linear component in its fall-off with $|z_3|$ for small and middle values of $|z_3|$. In fact, a linear exponential factor $Z(z_3^2) \sim e^{-c|z_3|/a}$ is expected as a manifestation of the nonperturbative effects generated by the straight-line gauge link.

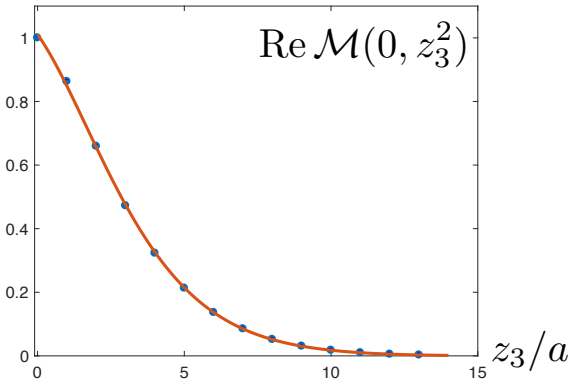


FIG. 6. Real part of the rest-frame density $\mathcal{M}(0, z_3^2)$

B. Reduced Ioffe-time distributions

In Fig. 7, we plot the results for the real part of the ratio $\mathcal{M}(Pz_3, z_3^2)/\mathcal{M}(0, z_3^2)$ as a function of z_3 taken at six fixed values of the momentum P. One can see that all the curves have a Gaussian-like shape. Thus, the $Z(z_3^2)$ link renormalization factor has been canceled in the ratio, as expected.

Furthermore, the curves look similar to each other, differing only by a decreasing width with P. In Fig. 8 , we plot the same data, but change the axis to $\nu = Pz_3$. As one can see, now the data practically fall on the same curve. For the imaginary part, the situation is similar.

This phenomenon corresponds to factorization of the x- and $k_\perp$-dependence for the soft TMD $\mathcal{F}(x, k_\perp^2)$, as discussed in previous sections.

C. Quark-antiquark decomposition

The real part of the Ioffe-time distribution is obtained from the cosine Fourier transform

$$\mathfrak{M}_R(\nu) \equiv \int_0^1 dx\, \cos(\nu x)\, q_v(x) \qquad (35)$$

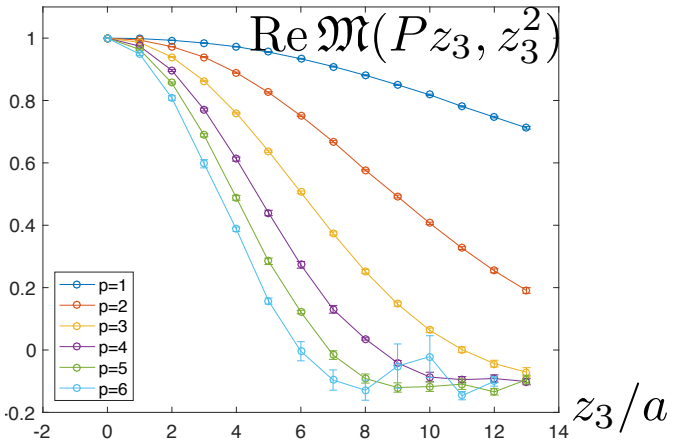


FIG. 7. Real part of the reduced distribution $\mathfrak{M}(Pz_3, z_3^2)$ plotted as a function of z_3. Here, $P = 2\pi p/L$.

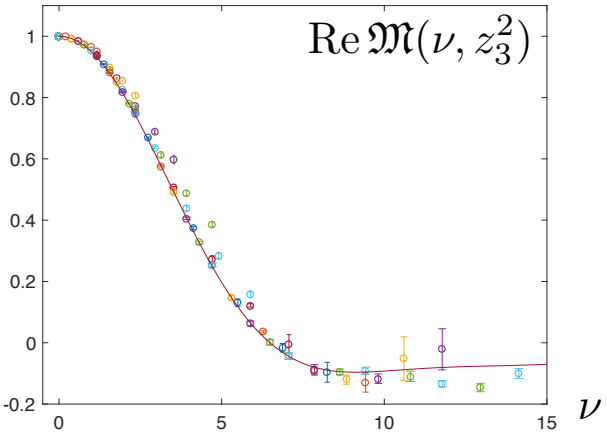


FIG. 8. Real part of $\mathfrak{M}(\nu, z_3^2)$ plotted as a function of $\nu = Pz_3$ and compared to the curve given by Eqs. (35), (36).

of the function $q_v(x)$ given by the difference $q_v(x) = q(x) - \bar{q}(x)$ of quark and antiquark distributions. In our case, q is $u - d$ and $\bar{q} = \bar{u} - \bar{d}$. The x-integral of $u - \bar{u}$ equals to the number of u-quarks in the proton, which is 2, while the x-integral of $d - \bar{d}$ equals 1. Thus, the x-integral of $q_v(x)$ should be equal to 1.

We found that our data for the real part are well described if one chooses the function

$$q_v(x) = \frac{315}{32}\sqrt{x}(1 - x)^3\,, \qquad (36)$$

whose x-integral is normalized to 1. To get it, we formed cosine Fourier transforms $\mathcal{M}(\nu; a, b)$ of the normalized $x^a(1 - x)^b$-type functions and found the parameters a, b by fitting our data. The comparison of the data with the curve based on Eqs. (35), (36) is shown in Fig. 8.

While all the data points were used in the fit, the latter is clearly dominated by the points with the smaller

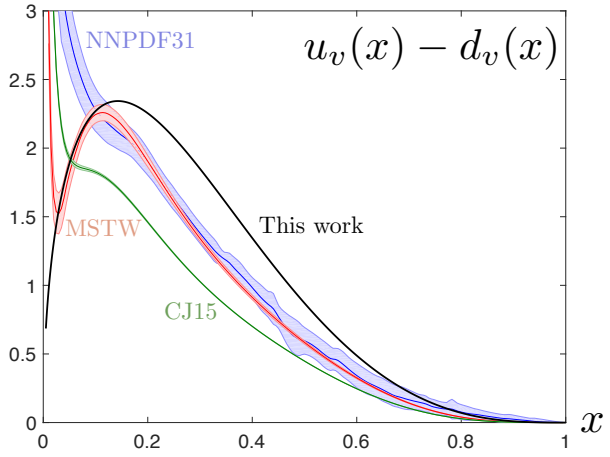


FIG. 9. Valence distribution $q_v(x)$ as given by Eq. (36) compared with the $Q^2 = 1$ GeV^2 NNLO global fits NNPDF31_nnlo_pch_as_0118_mc_164 [24] and MSTW2008nnlo68cl_nf4 [25]; and the NLO global fit CJ15nlo [26], all extracted using the LHAPD6 library [27]. The bands around the global fits indicate their experimental and systematic uncertainties.

values of Re $\mathfrak{M}(\nu, z_3^2)$. For $\nu < 10$, the data points lying above the curve, correspond to values of $z_3 = 3a$ to $5a$. As we will see later, they reflect the perturbative evolution: Re $\mathfrak{M}(\nu, z_3)$ increases when z_3 decreases. In this context, the overall curve (36) corresponds to PDF "at low normalization point", i.e., in the region, where the perturbative evolution stops.

In general, it is more appropriate to fit Re $\mathfrak{M}(\nu, z_3^2)$ as a function of two variables, ν and z_3, even though the dependence on z_3 is rather weak and noticeable just for a few points. Since we made a fit of Re $\mathfrak{M}(\nu, z_3)$ as a function of just one variable ν, there are points that visibly deviate from the curve, but we do not think that it makes sense to translate the evolution z_3-dependence of small-z_3 points into an error band to our curve in Fig. 8. In the Section V.D, we evolve the data points to a common reference scale $z_0 = 2a$ and show the error band for the results obtained in this way.

We realize that our lattice setup is rather crude (quenched approximation, very large pion mass), and for this reason we do not attempt to perform a thorough comparison of our results with experimental data. Still, we think that some kind of comparison is rather useful as an illustration.

Thus, we compare our $q_v(x)$ with three global fits for the difference $u_v(x) - d_v(x)$ of the valence distributions, see Fig. 9. These global fits curves correspond to $\mu = 1$ GeV scale, while our "low normalization point" curve corresponds to $\mu \lesssim 0.3$ GeV. Still, one can see that our curve is not very far from the NNPDF31 [24] NNLO fit down to $x = 0.1$ and from the MSTW [25] NNLO fit down to $x = 0.05$. We also show the NLO fit CJ15 [26].

Since the areas under each curve are equal to 1, our curve compensates the strong deficiency in the $x < 0.1$ region by exceeding the NNLO curves at $x > 0.1$ values.

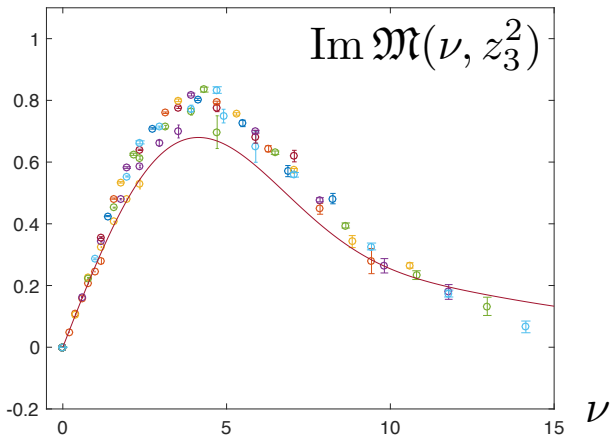


FIG. 10. Imaginary part of $\mathfrak{M}(\nu, z_3^2)$ compared to the curve $\mathfrak{M}_I^v(\nu)$ based on $\bar{q}(x) = 0$.

In other words, if our curve would better describe data in the $x < 0.1$ region, it would necessarily be smaller in the $x > 0.1$ region.

The sine Fourier transform

$$\mathfrak{M}_I(\nu) \equiv \int_0^1 dx\, \sin(\nu x)\, q_+(x) \tag{37}$$

is built from the function $q_+(x) = q(x) + \bar{q}(x)$, which may be also represented as $q_+(x) = q_v(x) + 2\bar{q}(x)$. If we neglect the antiquark contribution and use $q_+(x) = q_v(x)$, we get the curve shown in Fig. 10 (call it $\mathfrak{M}_I^v(\nu)$). The agreement with the data is strongly improved if we use a non-vanishing antiquark contribution, namely

$$\bar{q}(x) = \bar{u}(x) - \bar{d}(x) = 0.07\,\left[20\,x(1-x)^3\right]\,, \tag{38}$$

see Fig. 11. This function was obtained by fitting the data for the difference Im $\mathfrak{M}(\nu, z_3^2) - \mathfrak{M}_I^v(\nu)$ by sine

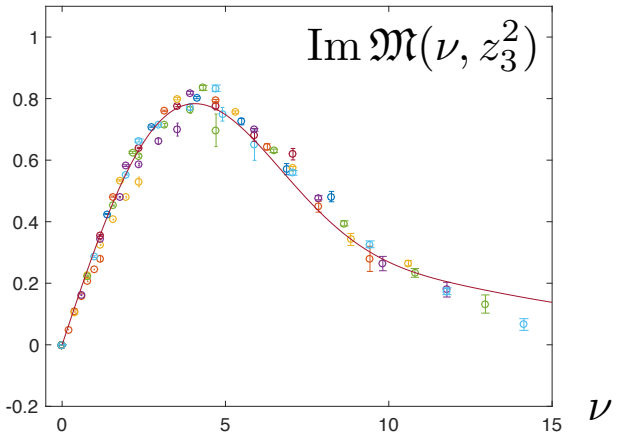


FIG. 11. Imaginary part of $\mathfrak{M}(\nu, z_3^2)$ compared to the curve based on $\bar{q}(x)$ given by Eq. (38).

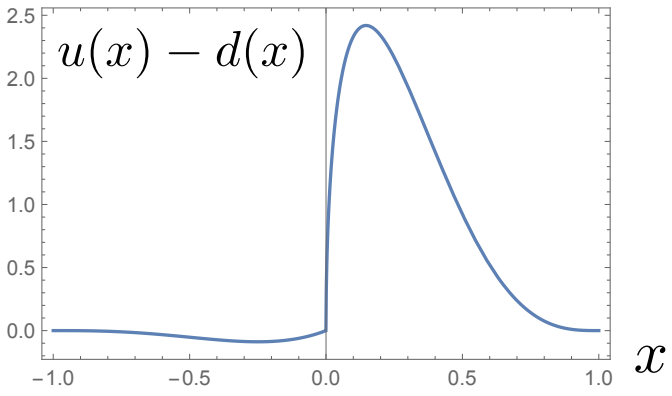


FIG. 12. Overall distribution $q(x)$ as defined by Eq. (40).

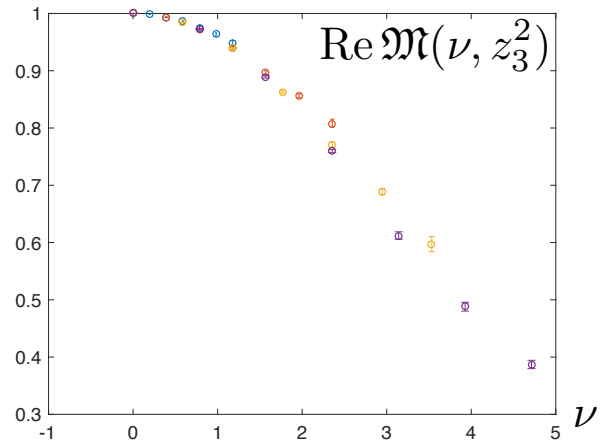


FIG. 13. Real part of $\mathfrak{M}(\nu, z_3^2)$ for $z_3/a = 1, 2, 3$, and 4.

Fourier transforms of $Ax^a(1-x)^b$ functions. This result corresponds to

$$\int_0^1 dx\,[\bar{u}(x) - \bar{d}(x)] = 0.07\ . \tag{39}$$

The combined distribution

$$\begin{aligned} q(x) &= u(x) - d(x) \\ &= [q_v(x) + \bar{q}(x)]\,\theta(x > 0) - \bar{q}(-x)\,\theta(x < 0) \end{aligned} \tag{40}$$

defined on the $-1 \le x \le 1$ interval is shown in Fig. 12.

D. Evolution

While an overall agreement of the data with a z_3-independent curve looks satisfactory, one can easily notice a residual z_3-dependence in the data. It is especially visible when, for a particular ν, there are several data points corresponding to different values of z_3. It is interesting to check if this dependence corresponds to perturbative evolution.

To begin with, the evolution of the real part should lead to its *decrease* when z_3^2 increases. On the other hand, as pointed out at the end of section III, the function $\mathrm{Im}\,\mathcal{M}(\nu, z_3^2)$ *increases* when z_3^2 *increases* as long as $\nu \lesssim 5.5$. Our data follow these patterns.

As we discussed, the evolution corresponds to $\ln z_3^2$ singularities of the Ioffe-time distributions for small z_3^2. Thus, a natural idea is to check if the data corresponding to small z_3' and z_3 may be related by

$$\mathfrak{M}(\nu, z'^2_3) = \mathfrak{M}(\nu, z_3^2) - \frac{2}{3}\frac{\alpha_s}{\pi}\ln(z_3'^2/z_3^2) B \otimes \mathfrak{M}(\nu, z_3^2) \tag{41}$$

for some value of α_s. Here B is the evolution kernel (21).

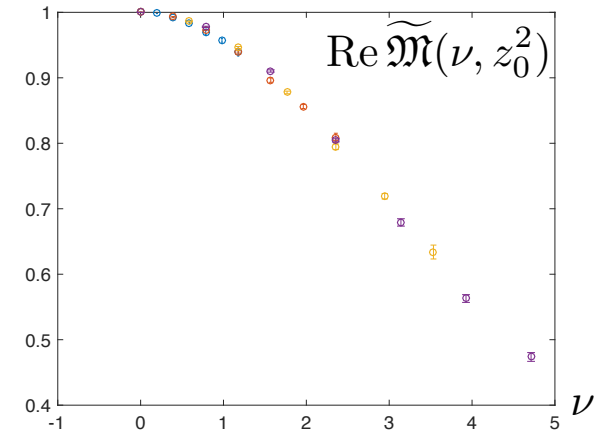


FIG. 14. Evolved data points for the real part.

In our case,

$$B \otimes \mathfrak{M}(\nu) = \int_0^1 du\,\frac{1+u^2}{1-u}\,[\mathfrak{M}(\nu) - \mathfrak{M}(u\nu)]. \tag{42}$$

More specifically, we fix the point z_3' at the value $z_0 = 2a$ corresponding, at the leading logarithm level, to the $\overline{\mathrm{MS}}$-scheme scale $\mu_0 = 1$ GeV and build the function

$$\widetilde{\mathfrak{M}}(\nu, z_0^2) \equiv \mathfrak{M}(\nu, z_3^2) - \frac{2}{3}\frac{\alpha_s}{\pi}\ln(z_0^2/z_3^2) B \otimes \mathfrak{M}(\nu, z_3^2) \tag{43}$$

from the data points for $\mathfrak{M}(\nu, z_3^2)$ using various values for α_s.

Since the perturbative evolution is expected for small z_3, we include in this analysis the data with z_3 up to 4 lattice spacings, which corresponds to energy scales $\mu = 2, 1, 0.7$ and 0.5 GeV.

For the real part, these data points are shown in Fig. 13. As one can see, there is a visible scatter of the

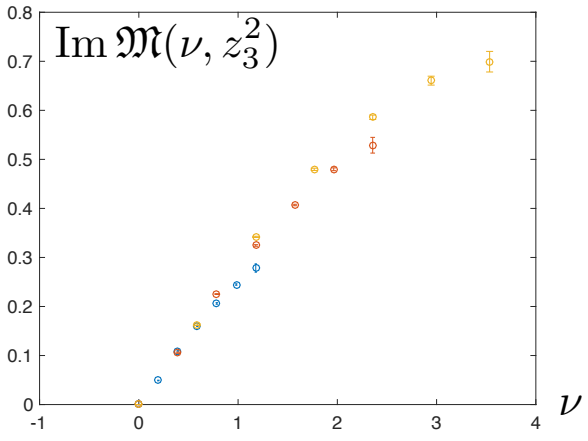


FIG. 15. Imaginary part of $\mathfrak{M}(\nu, z_3^2)$ for $z_3/a = 1, 2, 3$, and 4.

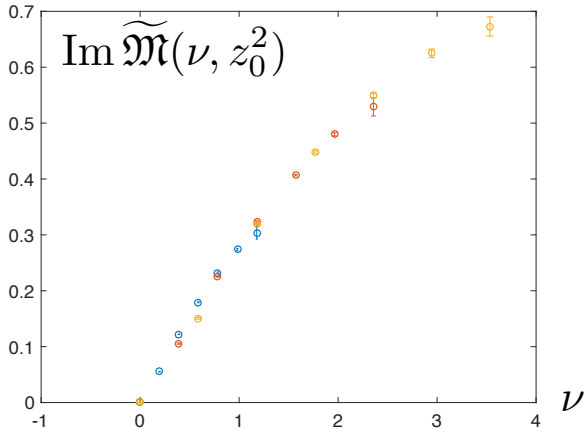


FIG. 16. Evolved data points for the imaginary part.

data points. Using $\alpha_s/\pi = 0.1$, we calculate the "evolved" data points corresponding to the function $\widetilde{\mathfrak{M}}(\nu, z_0^2)$. The results are shown in Fig. 14. The evolved data points are now very close to a universal curve.

In Fig. 15, we show the initial data points for the imaginary part. The evolved data points constructed using the same $\alpha_s/\pi = 0.1$ value are shown in Fig. 16. Again, they are close to a universal curve. This analysis indicates that the residual z_3^2-dependence of $\mathfrak{M}(\nu, z_3^2)$ at fixed ν is compatible with the expected logarithmic evolution at small z_3^2. Clearly this is an important feature of our calculation which needs to be further studied as it will play an essential role in reliable extraction of renormalized PDFs from this type of lattice calculations.

With a smaller lattice spacing, the use of perturbative evolution may be justified in a wider region of ν. While our data extend to rather large separations ~ 1 fm, we find it instructive to use them as an example to illustrate the trends generated by the perturbative evolution.

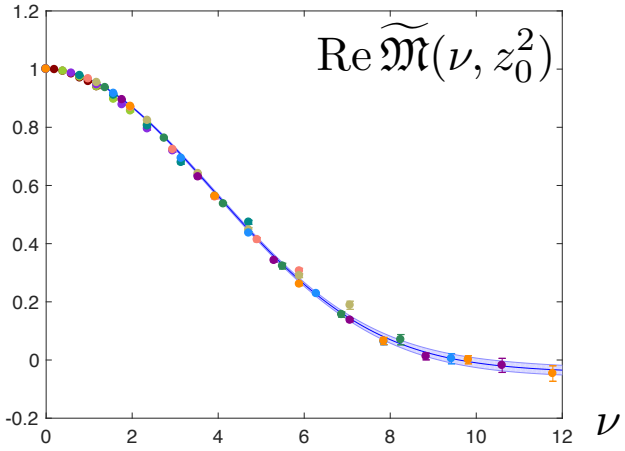


FIG. 17. Data points for Re $\mathfrak{M}(\nu, z_3^2)$ with $z_3 \leq 10a$ evolved to $z_0 = 2a$ as described in the text.

To this end, we applied the leading logarithm formula (43) with $z_0 = 2a$ and $\alpha_s/\pi = 0.1$ to our data points with $z_3 \leq 6a$. Assuming that evolution stops for $z_3 \gtrsim 6a$ (as indicated by our data), the data points with $7a \leq z_3 \leq 10a$ were evolved to z_0 using Eq. (43) with $z_3 = 6a$. The data points evolved in this way are shown in Fig. 17.

Fitting the evolved points by cosine Fourier transforms $\mathcal{M}(\nu; a, b)$ of the normalized $N(a, b)x^a(1-x)^b$-type functions, we found that they may be described if one takes $a = 0.36(6)$ and $b = 3.95(22)$. Treating $z_0 = 2a$ as the $\overline{\text{MS}}$ scale $\mu = 1$ GeV, one can further evolve the curve to

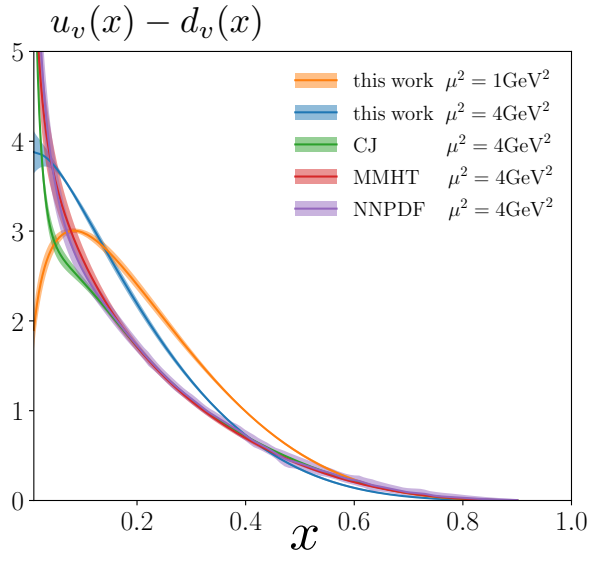


FIG. 18. Curve for $u_v(x) - d_v(x)$ built from the evolved data shown in Fig. 17, and treated as corresponding to the $\mu^2 = 1$ GeV^2 scale; then evolved to the reference point $\mu^2 = 4$ GeV^2 of the global fits.

the standard reference scale $\mu^2 = 4$ GeV^2 of the global fits, see Fig. 18. Comparing with Fig. 9, we see that the perturbative evolution shifts our curves, moving them closer to the global fits.

VI. SUMMARY

In this paper, we demonstrated a new method of extracting parton distributions from lattice calculations. It is based on the ideas, formulated in Ref. [11].

First, we treat the generic equal-time matrix element as a function $\mathcal{M}(\nu, z_3^2)$ of the Ioffe time $\nu = Pz_3$ and the distance z_3. The next idea is to form the ratio $\mathfrak{M}(\nu, z_3^2) \equiv \mathcal{M}(\nu, z_3^2)/\mathcal{M}(0, z_3^2)$ of the Ioffe-time distribution $\mathcal{M}(\nu, z_3^2)$ and the rest-frame density given by $\mathcal{M}(0, z_3^2)$.

Our lattice calculation clearly shows the presence of a linear component in the z_3-dependence of the rest-frame function, that may be attributed to the expected $Z(z_3^2) \sim e^{-c|z_3|/a}$ behavior generated by the gauge link. On the next step, we observe that the ratio $\mathcal{M}(Pz_3, z_3^2)/\mathcal{M}(0, z_3^2)$ has a Gaussian-type behavior with respect to z_3 for all 6 values of P that were used in the calculation. This means that $Z(z_3^2)$ factors entering into the numerator and denominator of the $\mathfrak{M}(Pz_3, z_3^2)$ ratio have been canceled, as expected.

Still, there is no *a priori* principle predicting that the remaining non-logarithmic z_3^2-dependence cancels between the numerator and the denominator of the ratio $\mathcal{M}(\nu, z_3^2)/\mathcal{M}(0, z_3^2)$. Such a z_3^2-dependence can be removed if needed with a systematic fitting procedure from which the Ioffe time PDF will be extracted in the $z_3^2 = 0$ limit.

However, we found that when plotted as a function of ν and z_3, the data both for the real and imaginary parts of $\mathfrak{M}(\nu, z_3^2)$ are very close to the respective universal functions. This observation indicates that the soft part of the z_3^2-dependence of $\mathcal{M}(\nu, z_3^2)$ has been canceled by the rest-frame density $\mathcal{M}(0, z_3^2)$. This phenomenon corresponds to factorization of the x- and $k_\perp$-dependence for the TMD $\mathcal{F}(x, k_\perp^2)$.

While this evidence in favor of the factorization property is an important result on its own, we want to stress that our approach *is not based* on the factorization. It is based on the use of the ratio $\mathcal{M}(\nu, z_3^2)/\mathcal{M}(0, z_3^2)$. Its residual soft z_3^2-dependence may be systematically analyzed and fitted, so that the z_3^2-limit may be taken in a controllable way.

Luckily, the data do not show a visible polynomial dependence on z_3^2 within our current statistical and systematic errors. In future work we intend to carefully study the residual polynomial z_3^2 effects and incorporate them in the extraction of PDFs using the lattice methodology introduced here.

In addition, we have checked that, for small $z_3 \leq 4a$, the residual z_3-dependence may be explained by perturbative evolution, with the α_s value corresponding to $\alpha_s/\pi = 0.1$. We have evolved these small-z_3 data points to the $z_3 = 2a$ scale, which corresponds to $\mu^2 = 1$ GeV^2. The evolved data better approximate universal curves both for real and imaginary parts of $\mathcal{M}$, supporting the argument that perturbative evolution is observed.

Thus, these $\nu \lesssim 4$ parts of the universal curves may be treated as corresponding to the $\mu = 1$ GeV scale. Other data points correspond to $z_3 > 4a$ values, and formally should be treated as corresponding to scales $\mu \lesssim 0.3$ GeV. All these data points basically lie on the same universal curve. This indicates that evolution stops at such scales. We compared this "low normalization point" curve with three global fits evolved to the $\mu = 1$ GeV scale, and observed that our curve (36) for the valence $u_v(x) - d_v(x)$ distribution shows the $(1-x)^3$ behavior for $x \to 1$ in accord with usual expectations. Also, it rather closely follows the NNPDF31 and, especially, MSTW NNLO global fits down to rather small x values.

Still, our curve strongly deviates from the global fits for $x < 0.1$ in the NNPDF31 case and for $x < 0.05$ in the MSTW case. However, the shape of PDFs is affected by the perturbative evolution. To illustrate the scope of these effects, we evolved all our points with $z_3 \leq 10a$ to a universal scale $z_0 = 2a$ corresponding to $\mu = 1$ GeV, and then further evolved the resulting PDF to $\mu = 2$ GeV, that is the standard reference scale for global fits. Our final curve is rather close to these fits, which demonstrates that the perturbative evolution plays an important role in comparison of lattice results with the data. Again, one needs smaller lattice spacings to justify the use of the perturbative evolution equation in a sufficiently wide interval of Ioffe time parameters ν.

The data also indicate a nonzero *positive* antiquark distribution $\bar{q}(x) = \bar{u}(x) - \bar{d}(x)$. It changes the x-integral of $q(x)$ by 7% and has $\sim x(1-x)^3$ behavior. Since we are using the quenched approximation, these antiquarks come from "connected diagrams". Hence, one should expect that the ratio $\bar{u}/\bar{d}$ *must* follow the flavor content of the proton, i.e. $\bar{u}/\bar{d} \sim 2$ and $\bar{u} > \bar{d}$. Our data agree with this expectation.

The present study has an exploratory nature, and its main goal was to develop techniques for lattice extraction of PDFs based on the ideas of Ref. [11]. Our results indicate that the basic method we put forward has a strong potential for obtaining reliable PDFs from lattice QCD. In future work we will refine our methods for incorporating evolution and controlling residual polynomial z_3^2 effects in the extraction of the Ioffe time distributions.

To achieve this, it is evident that smaller lattice spacings are required as well as a larger range of nucleon momenta. Furthermore, we need to study finite volume effects as well as to incorporate dynamical fermions with pion masses closer to the physical point. We plan to address all these issues in our future work.

ACKNOWLEDGMENTS

One of us (A.R.) thanks V. Braun and X. Ji for discussions and comments. We are very grateful to Nobuo Sato who performed the numerical evolution of the data as described in Sec. V and provided Fig. 18, and we are also indebted to him for the help in comparison of our results with global fits. This work is supported by Jefferson Science Associates, LLC under U.S. DOE Contract #DE-AC05-06OR23177. K.O. was supported in part by U.S. DOE grant #DE-FG02-04ER41302, and A.R. was supported in part by U.S. DOE Grant #DE-FG02-97ER41028. S.Z. acknowledges support by the National Science Foundation (USA) under grant PHY-1516509. This work was performed in part using computing facilities at the College of William and Mary which were provided by contributions from the National Science Foundation (MRI grant PHY-1626177), the Commonwealth of Virginia Equipment Trust Fund and the Office of Naval Research. In addition, this work used resources at NERSC, a DOE Office of Science User Facility supported by the Office of Science of the U.S. Department of Energy under Contract #DE-AC02-05CH11231.

[1] R. P. Feynman, *Photon-hadron interactions,* Reading 1972, 282p
[2] X. Ji, Phys. Rev. Lett. **110**, 262002 (2013).
[3] H. W. Lin, J. W. Chen, S. D. Cohen and X. Ji, Phys. Rev. D **91**, 054510 (2015).
[4] J. W. Chen, S. D. Cohen, X. Ji, H. W. Lin and J. H. Zhang, Nucl. Phys. B **911**, 246 (2016).
[5] C. Alexandrou, *et al.*, Phys. Rev. D **92**, 014502 (2015).
[6] J. H. Zhang, J. W. Chen, X. Ji, L. Jin and H. W. Lin, Phys. Rev. D **95**, no. 9, 094514 (2017).
[7] A. Radyushkin, Phys. Lett. B **767**, 314 (2017).
[8] A. V. Radyushkin, Phys. Rev. D **95**, no. 5, 056020 (2017).
[9] A. V. Radyushkin, Phys. Lett. B **735**, 417 (2014).
[10] A. V. Radyushkin, Phys. Rev. D **93**, no. 5, 056002 (2016).
[11] A. V. Radyushkin, Phys. Rev. D **96**, no. 3, 034025 (2017).
[12] B. L. Ioffe, Phys. Lett. **30B**, 123 (1969).
[13] V. Braun, P. Gornicki and L. Mankiewicz, Phys. Rev. D **51**, 6036 (1995).
[14] A. V. Radyushkin, Phys. Lett. **131B**, 179 (1983).
[15] M. Anselmino, M. Boglione, J. O. Gonzalez Hernandez, S. Melis and A. Prokudin, JHEP **1404**, 005 (2014).
[16] T. Ishikawa, Y. Q. Ma, J. W. Qiu and S. Yoshida, arXiv:1609.02018 [hep-lat].
[17] B. U. Musch, P. Hagler, J. W. Negele and A. Schäfer, Phys. Rev. D **83**, 094507 (2011).
[18] M. Luscher, S. Sint, R. Sommer, P. Weisz and U. Wolff, Nucl. Phys. B **491**, 323 (1997).
[19] S. Necco and R. Sommer, Nucl. Phys. B **622**, 328 (2002).
[20] C. Bouchard, C. C. Chang, T. Kurth, K. Orginos and A. Walker-Loud, Phys. Rev. D **96**, no. 1, 014504 (2017).
[21] E. Berkowitz *et al.*, arXiv:1704.01114 [hep-lat].
[22] B. C. Tiburzi *et al.*, Phys. Rev. D **96**, no. 5, 054505 (2017).
[23] P. E. Shanahan *et al.*, Phys. Rev. Lett. **119**, no. 6, 062003 (2017).
[24] R. D. Ball *et al.* [NNPDF Collaboration], Eur. Phys. J. C **77**, no. 10, 663 (2017)
[25] A. D. Martin, W. J. Stirling, R. S. Thorne and G. Watt, Eur. Phys. J. C **63**, 189 (2009).
[26] A. Accardi, L. T. Brady, W. Melnitchouk, J. F. Owens and N. Sato, Phys. Rev. D **93**, no. 11, 114017 (2016).
[27] A. Buckley, J. Ferrando, S. Lloyd, K. Nordström, B. Page, M. Rüfenacht, M. Schönherr and G. Watt, Eur. Phys. J. C **75**, 132 (2015).